Evidence of transverse wobbling motion in ^{151}Eu

A. Mukherjee,[1] S. Bhattacharya,[2] T. Trivedi,[1,3,*] S. Tiwari,[3] R. P. Singh,[4] S. Muralithar,[4] Yashraj,[4] K. Katre,[4] R. Kumar,[4] R. Palit,[5] S. Chakraborty,[6] S. Jehangir,[7,8] Nazira Nazir,[7,9] S. P. Rouoof,[8] G. H. Bhat,[7] J. A. Sheikh,[9] N. Rather,[8] R. Raut,[10] S. S. Ghugre,[10] S. Ali,[11] S. Rajbanshi,[12] S. Nag,[13] S. S. Tiwary,[14] A. Sharma,[15] S. Kumar,[16] S. Yadav,[17] and A. K. Jain[2]

[1]*Department of Pure & Applied Physics, Guru Ghasidas Vishwavidyalaya, Koni, Bilaspur-495009, India*
[2]*Amity Institute of Nuclear Science & Technology, Amity University U.P., Noida-201313, India*
[3]*Department of Physics, University of Allahabad, Prayagraj- 211002, India*
[4]*Inter University Accelerator Centre, Aruna Asaf Ali Marg, New Delhi-110067, India*
[5]*Department of Nuclear and Atomic Physics,Tata Institute of Fundamental Research, Mumbai-400005, India*
[6]*Variable Energy Cyclotron Centre, Kolkata-700064, India*
[7]*Department of Physics, S.P. College, Srinagar, Jammu and Kashmir, 190 001, India*
[8]*Department of Physics, Islamic University of Science and Technology, Jammu and Kashmir, 192 122, India*
[9]*Department of Physics, University of Kashmir, Hazratbal, Srinagar, 190 006, India*
[10]*UGC-DAE Consortium for Scientific Research Centre, Kolkata-700106, India*
[11]*Government General Degree College at Pedong, Kalimpong-734311, India*
[12]*Department of Physics, Presidency University, Kolkata-700073, India*
[13]*Department of Physics, IIT(BHU), Varanasi-221005, India*
[14]*Department of Physics, Manipal university Jaipur, Rajasthan-303007, India*
[15]*Department of Physics, Himachal Pradesh University, Shimla 171005, India*
[16]*Department of Physics and Astrophysics, University of Delhi, Delhi-110007, India*
[17]*Department of Physics, Panjab University, Chandigarh-160014, India*

(Received 21 December 2022; revised 22 January 2023; accepted 8 May 2023; published 22 May 2023)

Transverse wobbling was investigated in the ^{151}Eu nucleus by populating the excited states using ^{148}Nd(^{7}Li, 4n) ^{151}Eu at a beam energy of 30 MeV. Three new interconnecting transitions have been placed between the two negative parity bands. The *M1*/*E2* character of the interconnecting $\Delta I = 1$ transitions between the negative parity bands was extracted from the mixing ratios using the R_{DCO} and linear polarization method. The spin and parity of the states of different bands have also been assigned. The dominant *E2* character of the interlinking transitions between the yrast and first phonon wobbling band and the dominant *M1* character between the yrast band and its signature partner band indicate the presence of transverse wobbling in the ^{151}Eu nucleus. It is further demonstrated that the triaxial projected shell model approach describes the observed experimental properties.

DOI: 10.1103/PhysRevC.107.054310

I. INTRODUCTION

The nonaxial or triaxial nucleus with uneven density distribution along its three principal axes, medium (m), long (l), and short (s) axes, is energetically favored to rotate around the principal axis having the largest moment of inertia (MoI), i.e., $\mathcal{J}_m \geqslant \mathcal{J}_l \neq \mathcal{J}_s$, respectively. The characteristic feature of such a triaxial nucleus is the presence of chiral rotation or wobbling motion. Initially, the wobbling motion of the even-even triaxially deformed nucleus was described by Bohr and Mottelson [1] without the inclusion of the intrinsic angular momentum. In case of the odd A nucleus, wobbling excitations can be induced from the alignment of high-*j* particles as explained by Hamamoto [2]. Further, Frauendorf and Dönau classified the wobbling motion of the triaxial nuclei into two categories viz. *longitudinal and transverse* wobbling [3]. The change in the pattern of wobbling energy (E_{wobb}) as a function of increasing spin is the primary criterion to distinguish between the two wobbling modes. The wobbling energy decreases (increases) with increasing spin for the transverse (longitudinal) wobbling mode. A triaxial nucleus showcases transverse wobbling motion when the quasiparticle (hole) emerging from the bottom (top) of a deformed shell aligns its angular momentum *j* with the *s* axis (*l* axis), whereas in the case of a longitudinal wobbler, the angular momentum of the odd particle aligns with the axis having the largest moment of inertia, i.e., the medium axis (*m*) [4].

The first experimental evidence of wobbling motion in the nucleus was observed in the ^{163}Lu isotope [5], which arises from the excitation of the wobbling phonon ($n_\omega = 1$) built on the aligned proton $i_{13/2}$ orbital. Following this breakthrough observation, one and (or) two phonon wobbling bands were simultaneously observed in the chain of odd mass Lu isotopes [6–9], ^{167}Ta [10], ^{135}Pr [11,12], ^{133}La [13], ^{127}Xe [14], ^{133}Ba [15], ^{183,187}Au [4,16], and ^{105}Pd [17] nuclei. Apart from these odd mass nuclei, ^{130}Ba [18,19] and ^{136}Nd [20,21] are the only two even-even nuclei in which wobbling motion was

*ttrivedi1@gmail.com

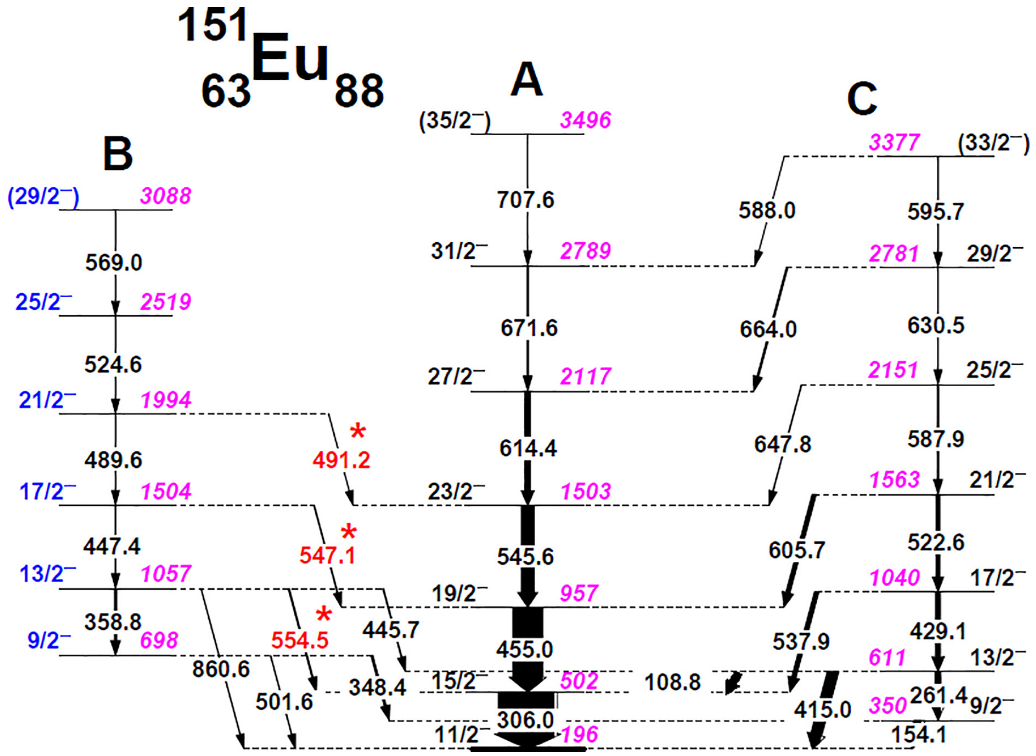

FIG. 1. Partial level scheme of ^{151}Eu based on the present work and the previous studies [31–34]. The newly observed transitions in the present work (labeled in red font) are marked by asterisks, while the spin states labeled in blue font are modified in the present study. The thick solid black line representing the $11/2^-$ state is an isomeric state with $\tau_{1/2} = 58.9(5)$ μs. The transition energies are in keV. The level energies are rounded off to the nearest keV.

observed to date. Among these nuclei, ^{127}Xe, ^{133}Ba, ^{133}La, and ^{187}Au fall into the category of longitudinal wobbling (LW), while the rest of them show the transverse mode of wobbling motion (TW). The wobbling phonon excitation with decaying $\Delta I = 1$ transitions between the strongly deformed bands are observed at a high spin range in Lu and Ta isotopes, whereas in other nuclei, these interlinking transitions are observed between two normal deformed bands lying within a spin range of 15–20$\hbar$. So far, multiphonon wobbling bands have been observed in ^{183}Au [16], ^{127}Xe [14], ^{135}Pr [12], and ^{133}Ba [15] nuclei where the wobbling excitations of the first three candidates is associated with particlelike behavior of the quasiparticles while the later showcases the observation of wobbling excitations from a holelike quasiparticle. Contemporarily, various theoretical interpretations have been made to evaluate the presence of wobbling motion in these nuclei [19,20,22–28]. On the one hand, the two-dimensional plots of the probability distributions of the spin coherent states (SCS) have been used to generalize the classification of the collective excitations of the quantum states of the particle coupled to a triaxial rotor (PTR) model as transverse and longitudinal wobbling modes [25]. On the other hand, another terminology called “tilted precession” (TiP) was proposed to interpret and classify the deformed bands observed in these triaxial nuclei [23]. However, based on different studies, the wobbling motion in some of the suggested wobblers is still under debate [23,27,29]. Recently, the theoretical prediction of wobbling excitation based on adiabatic and configuration-fixed constrained triaxial CDFT calculations in $^{57-62}$Ni isotopes opens up $A \approx 60$ mass region for studying the presence of wobbling phenomenon [30].

Although the wobbling motion of a nucleus was studied in the ∼130 and 180 mass region, such evidence is yet to be observed in the ∼150 mass region. The collective structures of the nuclei lying in the ∼150 mass region have been rigorously studied in the past decades. For instance, Jongman *et al.* had established the reflection asymmetric structure of the ^{151}Eu isotope by observing enhanced *E1* transitions between its positive and negative parity bands [32]. The previous study of ^{151}Eu has also reported the presence of strong interband $\Delta I = 1$ transitions which are interpreted to arise from the rotation of the triaxial shape [32]. The theoretical particle rotor calculation with the odd proton in deformed potential points towards the triaxial shape of the nucleus with $\epsilon_2 \sim 0.19$ at $\gamma = 20^\circ$; however, because of the limitation of the model, the calculated level energies were not much sensitive to the chosen deformation parameters [33]. Further, the similarity between the ratio of transition strength compared with the neighboring triaxial ^{150}Ho, also indicates its nonaxial structure [32], however, concrete evidence is yet to be found supporting such a triaxial structure.

In the present work, we have studied the triaxial structure of ^{151}Eu by performing detailed in beam γ-ray spectroscopic measurement. The band built on the unfavored sequence of the yrast band in the ^{151}Eu nucleus is predicted to arise because of the one-phonon wobbling excitation along with the identification of the signature partner (SP) band for the first time in ∼150 mass region. The ambiguity in spin and the parity of the signature partner band was removed on the basis of the directional correlation of oriented nuclei ratio and polarization measurement. The nature of the mixed interlinking transitions has also been established using these methods to determine the dominant $M1/E2$ character of the transitions. Further, the triaxial projected shell model (TPSM) analysis was performed to interpret the experimental results.

II. EXPERIMENTAL DETAILS

The excited states of ^{151}Eu were studied using the ^{148}Nd(^{7}Li, 4n) ^{151}Eu fusion evaporation reaction and Indian National Gamma Array (INGA) [35] at IUAC, New Delhi. The 30-MeV energetic beam of ^{7}Li, provided by 15 UD pelletron was bombarded on ^{148}Nd target of thickness 750 μg backed with 12 mg/cm^2 of ^{197}Au. The decaying γ rays were detected using 16 Compton suppressed clover detectors placed at 32°, 57°, 90°, 123°, and 148° along with two ancillary LEPS detectors at 61° and 119°, respectively. The relative efficiency and energy calibration of the detection system were performed with the two radioactive sources ^{152}Eu and ^{133}Ba by placing them at the target position. The coincidence data was sorted in different symmetric and angle-dependent asymmetric $\gamma - \gamma$ matrices using the INGASORT program [36]. The $\gamma - \gamma$ matrices were analyzed using the RADWARE [37,38] and ROOT [39] software packages. Further, an asymmetric matrix consisting of events detected by the clover detectors at 148° on one axis and 90° on the other axis was constructed to assign the multipolarities of the γ rays based on the directional correlation of oriented nuclei (DCO) ratio measurements. A total of 5.2×10^8 γ-γ coincidence events were collected in event-by-event mode.

III. DATA ANALYSIS

A. Level scheme

The partial level scheme of ^{151}Eu nucleus relevant to the present study is shown in Fig. 1. The negative parity yrast band A emerges from an isomer, having lifetime $\tau_{1/2} = 58.9(5)$ μs, at $11/2^-$ state [32] and was observed up to the $(35/2^-)$ state at level energy 3496 keV. The band C was observed up to the $33/2^-$ state at an excitation energy of 3377 keV. The spin and parity of the negative parity bands A and C are consistent with the previous studies [32,33]. The ambiguity in the spin and parity of band B in the previous work [32] was removed in the present work by performing the $R_{\rm DCO}$ and polarization measurements. The previously reported $7/2^-$ state at 243-keV excitation energy in band B with $\tau_{1/2} = 0.36(2)$ ns [34] is not observed in the present study. The band B was observed up to the $(29/2^-)$ state, and three new interconnecting γ-ray transitions with energies 554.5, 547.1, and 491.2 keV have been identified and placed between bands A and B. The representative gated spectra at 306.0- and 524.6-keV transitions are shown in Figs. 2 and 3, respectively, to support the placement of these interlinking transitions. The intensities of the observed transitions in bands A, B, and C are measured with respect to the 306.0-keV transition, as listed in Table I. The intensity uncertainties include systematic errors which are estimated to be 5% for $200 \leqslant E_\gamma \leqslant 1000$ keV and 10% for energies outside of this range.

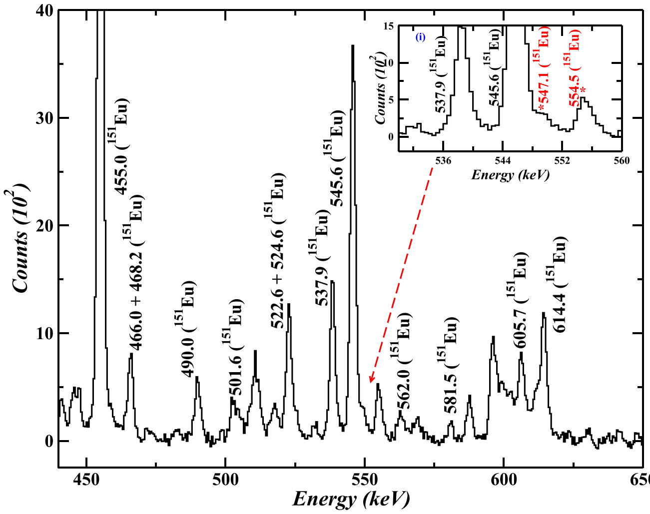

FIG. 2. A portion of the background subtracted spectrum obtained by gating on 306.0-keV transition of band A in ^{151}Eu. The red colored asterisk marked energies denote the newly placed transitions in the level scheme.

B. Angular correlation and polarization measurements

The assignment of the spin and parity of the γ-ray transitions was done using the directional correlation of oriented states (DCO) ratio, and linear polarization measurements, respectively. In the present study, the DCO ratio is defined as

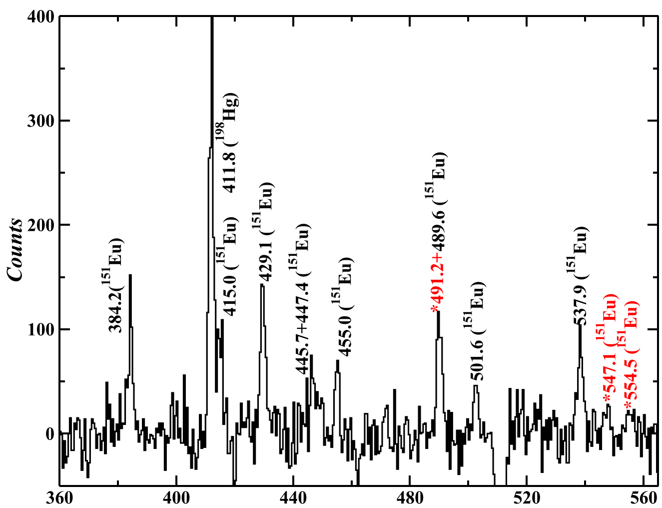

FIG. 3. A portion of the background subtracted spectrum obtained by gating on 524.6-keV transition of band B in ^{151}Eu. The red colored asterisk marked energies denote the newly placed transitions in the level scheme. The 411.8-keV transition originates from the ^{198}Hg nucleus as it was populated because of the reaction of the ^{7}Li beam on ^{197}Au backing.

TABLE I. Excitation energies (E_i) of levels, spin-parity assignments for the initial (I_i^π) and final (I_f^π) state, γ-ray transition energies ($E\gamma$), relative intensities ($I\gamma$), DCO ratios (R_{DCO}), polarization asymmetries ($\triangle$), mixing ratios (δ), and multipolarities of the γ rays observed in the decay of ^{151}Eu.

E_i(keV)	$(I_i^\pi) \rightarrow (I_f^\pi)$	E_γ(keV)[a]	I_γ	R_{DCO}	$\triangle$	δ[b]	δ[c]	δ_{av}	Assignment
350	$9/2^- \rightarrow 11/2^-$	154.1	13.8(7)	0.65(12)	–	–	–	–	$(M1/E2)$
502	$15/2^- \rightarrow 11/2^-$	306.0	100	0.97(11)	0.160(24)	–	–	–	$E2$
611	$13/2^- \rightarrow 15/2^-$	108.8	10.5(6)	0.68(10)	–	–	–	–	$(M1/E2)$
611	$13/2^- \rightarrow 9/2^-$	261.4	9.5(5)	0.98(16)	–	–	–	–	$(E2)$
611	$13/2^- \rightarrow 11/2^-$	415.0	19.3(10)	0.44(7)	0.038(35)	-3.3^{+9}_{-14}	-3.3^{+13}_{-30}	-3.3^{+15}_{-33}	$M1/E2$
698	$9/2^- \rightarrow 11/2^-$	501.6	1.0(1)	0.61(11)	–	–	–	–	$(M1/E2)$
698	$9/2^- \rightarrow 9/2^-$	348.4	3.7(3)	–	–	–	–	–	–
957	$19/2^- \rightarrow 15/2^-$	455.0	52.8(27)	1.02(11)	0.222(20)	–	–	–	$E2$
1040	$17/2^- \rightarrow 13/2^-$	429.1	8.9(7)	0.97(15)	0.227(55)	–	–	–	$E2$
1040	$17/2^- \rightarrow 15/2^-$	537.9	7.9(5)	0.54(9)	0.024(15)	-6.2^{+25}_{-88}	-6.3^{+33}_{-88}[d]	-6.3^{+41}_{-88}	$M1/E2$
1057	$13/2^- \rightarrow 9/2^-$	359.0	1.6(1)	0.96(17)	–	–	–	–	$(E2)$
1057	$13/2^- \rightarrow 13/2^-$	445.7	1.7(1)	0.84(18)	–	–	–	–	$\Delta I = 0, M1/E2$
1057	$13/2^- \rightarrow 15/2^-$	554.5	2.4(3)	0.68(10)	−0.079(28)	-0.08^{+10}_{-9}	-0.10^{+2}_{-11}	-0.09^{+11}_{-14}	$M1/E2$
1057	$13/2^- \rightarrow 11/2^-$	860.6	0.9(1)	–	–	–	–	–	–
1503	$23/2^- \rightarrow 19/2^-$	545.6	22.6(13)	1.02(12)	0.200(36)	–	–	–	$E2$
1504	$17/2^- \rightarrow 13/2^-$	447.4	1.5(1)	1.05(17)	–	–	–	–	$(E2)$
1504	$17/2^- \rightarrow 19/2^-$	547.1	1.5(1)	–	–	–	–	–	–
1563	$21/2^- \rightarrow 17/2^-$	522.6	6.9(5)	0.92(13)	–	–	–	–	$(E2)$
1563	$21/2^- \rightarrow 19/2^-$	605.7	7.5(5)	0.56(11)	–	–	–	–	$(M1/E2)$
1994	$21/2^- \rightarrow 17/2^-$	489.6	1.2(1)	0.96(13)	–	–	–	–	$(E2)$
1994	$21/2^- \rightarrow 23/2^-$	491.2	<0.5	–	–	–	–	–	–
2117	$27/2^- \rightarrow 23/2^-$	614.4	10.0(6)	0.95(14)	–	–	–	–	$(E2)$
2151	$25/2^- \rightarrow 21/2^-$	587.9	2.8(2)	0.95(18)	–	–	–	–	$(E2)$
2151	$25/2^- \rightarrow 23/2^-$	647.8	1.2(1)	–	–	–	–	–	–
2519	$25/2^- \rightarrow 21/2^-$	524.6	1.1(1)	0.91(25)	–	–	–	–	$(E2)$
2781	$29/2^- \rightarrow 27/2^-$	664.0	2.6(2)	0.59(10)	–	–	–	–	$(M1/E2)$
2781	$29/2^- \rightarrow 25/2^-$	630.5	<0.5	–	–	–	–	–	–
2789	$31/2^- \rightarrow 27/2^-$	671.6	2.5(2)	1.06(22)	–	–	–	–	$(E2)$
3088	$(29/2^-) \rightarrow 25/2^-$	569.0	0.7(1)	–	–	–	–	–	–
3377	$(33/2^-) \rightarrow 29/2^-$	595.7	1.6(2)	–	–	–	–	–	–
3377	$(33/2^-) \rightarrow 31/2^-$	588.0	< 0.1	–	–	–	–	–	–
3496	$(35/2^-) \rightarrow 31/2^-$	707.6	< 0.1	–	–	–	–	–	–

[a]The uncertainty in the E_γ values is 0.5 keV.
[b]mixing ratio obtained from R_{DCO} method in the present study.
[c]mixing ratio obtained from R_{DCO}-polarization method in the present study.
[d]The maximum probable negative uncertainty is mentioned for 537.9 keV.

[40]

$$R_{\mathrm{DCO}} = \frac{I_{\gamma 1} \text{ observed at } 148^\circ \text{ gated on } \gamma_2 \text{ at } 90^\circ}{I_{\gamma 2} \text{ observed at } 90^\circ \text{ gated on } \gamma_2 \text{ at } 148^\circ}, \quad (1)$$

where the I_γ denotes the intensity of the γ rays. The value of R_{DCO} depends on the detector geometry as well as the substate population width (σ/j) of the fusion evaporation reaction which is derived from the experimentally observed pure *E2* and *E1* transitions. In the present experimental setup, the R_{DCO} values of stretched *E1* transitions (384.2, 466.0, 587.2 keV) from the residual nuclei (^{151}Eu and ^{198}Hg) were compared with the theoretically calculated R_{DCO} for different values of σ/j using the ANGCOR [41] program. The comparison between the theoretical and experimentally observed R_{DCO} estimates the average value of $\sigma/j \approx 0.35$. Thus, for the present geometrical setup $R_{\mathrm{DCO}} \approx 1$ for stretched quadrupole transitions and $R_{\mathrm{DCO}} \approx 0.6$ for stretched dipole transitions when the gate is on the stretched quadrupole transition, whereas the R_{DCO} for mixed transitions differ from these values depending on their mixing ratios (δ). The R_{DCO} values obtained in the present study are listed in Table I. The spin assignment of the states in signature partner band B with band head at 698-keV level energy was ambiguous in the previous study [32]. In the present work, the spin of these states was confirmed and modified on the basis of the R_{DCO} values of the corresponding deexciting transitions. The spin of the state with the 698-keV-level energy was changed to $9/2^-$ from $(11/2^-)$ [32] based on the $R_{\mathrm{DCO}} = 0.61(11)$ of the decaying 501.6-keV transition, interlinking band B with the $h_{11/2}$ band A. Further, the $R_{\mathrm{DCO}} = 0.68(10)$ of 554.5 keV shows the dipole nature of the transition confirming the $13/2^-$ spin state of 1057-keV-level energy. The quadrupole nature of intraband 359.0-keV transition in band B with $R_{\mathrm{DCO}} = 0.96(17)$ further supports the assignment of the $9/2^-$ and $13/2^-$ spins to 698- and 1057-keV-level energies, respectively. Moreover, the $R_{\mathrm{DCO}} = 1.05(17)$, 0.96(13), and 0.91(25) of the

TABLE II. The deduced polarization [$P(\theta)$], measured polarization asymmetries ($\triangle$), and calculated polarization sensitivity (Q) of the gamma rays produced in the experiment. The angular distribution coefficients (a_2 and a_4) were taken from Refs. [45,31] for ^{198}Hg and ^{151}Eu, respectively.

Nucleus	E_γ(keV)	a_2	a_4	$P(\theta)$	$\triangle$	Q
^{198}Hg	411.8	0.23(2)	−0.05(2)	0.36(3)	0.131(9)	0.36(3)
^{151}Eu	455.3	0.37(8)	−0.04(6)	0.66(7)	0.222(20)	0.34(7)
^{198}Hg	587.2	−0.20(3)	−0.05(3)	0.27(4)	0.080(26)	0.29(5)
^{198}Hg	636.6	0.24(2)	−0.03(2)	0.39(3)	0.094(8)	0.24(3)
^{198}Hg	767.3	0.26(3)	−0.08(4)	0.40(5)	0.079(29)	0.20(6)

intraband 447.4-, 489.6-, and 524.6-keV transitions, respectively, in band B also indicate their quadrupole nature. Apart from this, the measured $R_{\mathrm{DCO}} = 0.44(7)$, 0.54(9), 0.56(11), and 0.59(10) values of the interconnecting 415.0-, 537.9-, 605.7-, and 664.0-keV transitions respectively, between the wobbling band C and yrast band A show their mixed dipole nature.

The assignment of the parity to the states was carried out using linear polarization measurements. The clover detectors placed at 90° angle act as a Compton polarimeter and are used to deduce the polarization asymmetry of the transitions. The polarization asymmetry ($\triangle$) is measured using the following formula:

$$\triangle = \frac{a(E_\gamma)N_\perp - N_\parallel}{a(E_\gamma)N_\perp + N_\parallel}, \quad (2)$$

where $N_\perp$ ($N_\parallel$) is the number of counts of γ-ray transitions lying perpendicular (parallel) to the plane formed by the beam direction and the direction of emission of gamma ray. The 1.03(7) value of the correction factor $a(E_\gamma)$ was measured using the decay data of the ^{152}Eu radioactive source in the present experimental setup. To determine the experimental asymmetry, two asymmetric matrices were constructed with coincidence events corresponding to parallel and perpendicular segments of the clover detectors (with respect to the emission plane) along one axis and coincident events corresponding to all the detectors of the array on the other axis [40,42]. Further, the polarization asymmetry ($\triangle$) is used along with the polarization sensitivity (Q) to determine the linear polarization of the γ- rays using the following formula [42,43]:

$$P(\theta) = \frac{\triangle}{Q}. \quad (3)$$

The polarization sensitivity Q is a measure to characterize a Compton polarimeter and is calculated using pure transitions from different residual nuclei populated in the present reaction. The sensitivity parameter was determined using Eq. (3), where the polarization asymmetry of the pure quadrupole and dipole transitions was obtained from the present analysis, as presented in Table II. The linear polarization $P(\theta)$ measurement was carried out using the Klein-Nishina formula [44] in which the angular distribution coefficients a_2 and a_4 parameters were taken from Refs. [31,45] for ^{198}Hg and ^{151}Eu, respectively. Figure 4 represents the fitted curve of the Q parameter using the following relation [43]:

$$Q = Q_0(a + b \times E_\gamma), \quad (4)$$

where Q_0 represents the polarization sensitivity of an ideal Compton polarimeter and is defined as

$$Q_0 = \frac{1+\alpha}{1+\alpha+\alpha^2}, \quad (5)$$

with $\alpha = \frac{E_\gamma(\mathrm{keV})}{511}$. The parameters a and b having the values of 0.626(125) and $-3.22(23) \times 10^{-4}$ are obtained from the least square-fitting method. A positive value of the linear polarization indicates the electric nature of the transition, while a negative value indicates the magnetic nature.

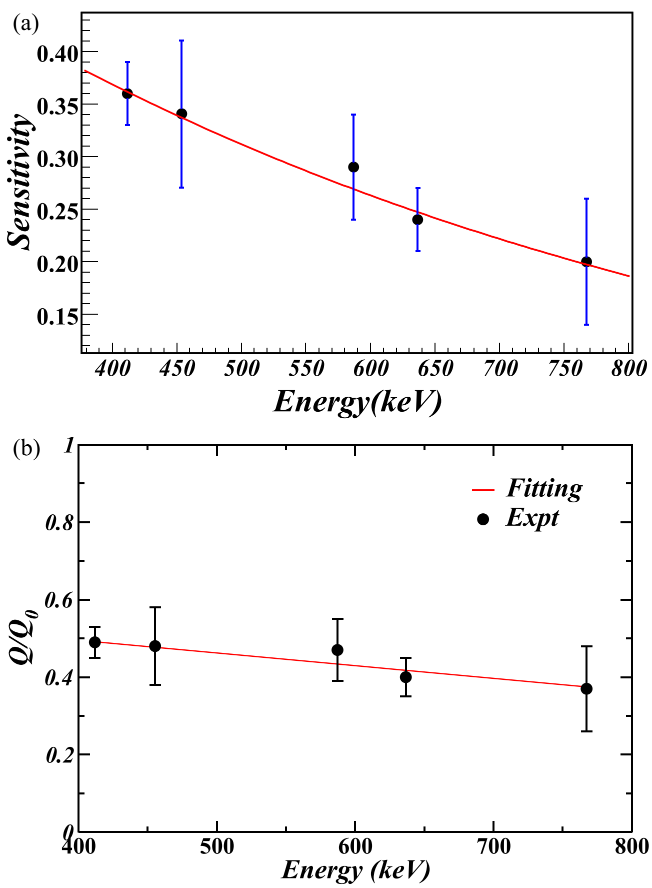

FIG. 4. (a) Polarization sensitivity of the clover detectors placed at 90° of the INGA array used in the experiment. (b) The variation of Q/Q_0 as a function of energy (in keV). The solid line represents the fitted curve of the experimental data points.

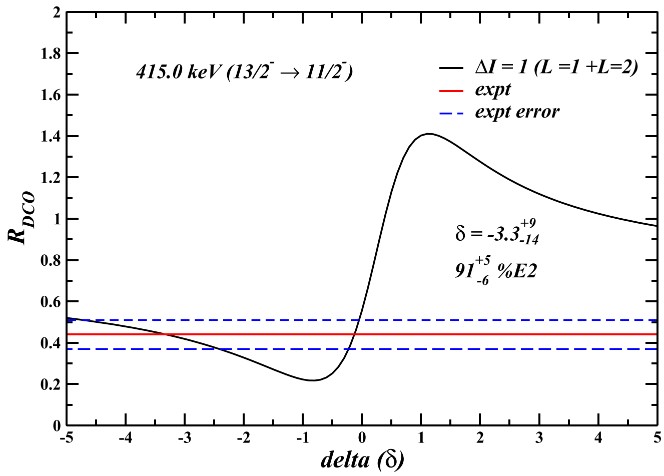

FIG. 5. The variation of $R_{\rm DCO}$ as a function of mixing ratio (δ) for 415.0-keV transition in ^{151}Eu giving two values of $\delta = -3.3^{+9}_{-14}$ and -0.12^{+8}_{-10}. The higher value of δ is mentioned in the plot as it is also supported by the polarization measurement.

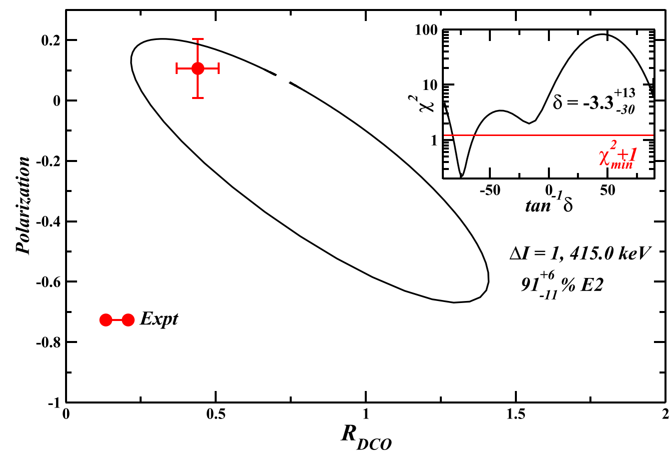

FIG. 6. The variation of $R_{\rm DCO}$ as a function of the polarization at different mixing ratio (δ) for 415.0-keV transition in ^{151}Eu in which the inset shows the minimum of the χ^2 versus $\tan^{-1}\delta$ plot giving mixing ratio $\delta = -3.3^{+13}_{-30}$.

In the present study, the tentative parity of band B has now been confirmed using polarization values. Table I shows the polarization asymmetry values of the γ-ray transitions. The negative parity was assigned to band B based on the polarization asymmetry of the new interlinking 554.5-keV transition between bands B and A. The negative value of $\triangle = -0.079(28)$ of 554.5-keV transition shows its dominant magnetic nature. While the positive values of $\triangle = 0.038(35)$ and 0.024(15) of the mixed $\Delta I = 1$ interconnecting transitions 415.0 and 537.9 keV between bands C and A indicate its dominant electric nature. The errors in linear polarization measurement have been determined from the error propagation method [42,46].

Further, the mixing ratios of the $\Delta I = 1$, $M1/E2$ interconnecting transitions have been extracted from the comparison of experimental and theoretical $R_{\rm DCO}$ values and the $R_{\rm DCO}$-polarization method. Figure 5 shows the theoretical $R_{\rm DCO}$ versus mixing ratio (δ) plot for 415.0-keV transition decaying from the $13/2^- \rightarrow 11/2^-$. The comparison of experimental $R_{\rm DCO}$ value of 415.0 keV gives two values of $\delta = -3.3^{+9}_{-14}$ and -0.12^{+8}_{-10}. The linear polarization supports the higher value of the mixing ratio. As shown in Fig. 6, the value of δ obtained from the $R_{\rm DCO}$-polarization method gives $\delta = -3.3^{+13}_{-30}$. Thus the average value of the mixing ratio for 415.0-keV transition obtained from both the methods is $\delta_{\rm av} = -3.3^{+15}_{-33}$. Notably, the experimental $\delta_{\rm av}$ value lies close to the $\delta = -5.6 \pm 26$, which is obtained from the angular distribution coefficients a_2 and a_4 taken from Ref. [31]. Similarly, the average mixing ratio $\Delta I = 1$, 537.9-keV transition, obtained using both $R_{\rm DCO}$ and the $R_{\rm DCO}$-polarization method (as shown in Figs. 7 and 8, respectively) is $\delta_{av} = -6.3^{+41}_{-88}$. The higher mixing ratio values suggest that the interlinking $\Delta I = 1$, 415.0-, and 537.9-keV transitions between bands A and C have dominant $E2$ characters. On the other hand, the $\delta_{\rm av} = -0.09^{+11}_{-14}$ of 554.5-keV transition between bands A and B (as obtained from Figs. 9 and 10) shows its dominant $M1$ character. The reduced χ^2 minimization, with three degrees of freedom, for the experimental $R_{\rm DCO}$ and polarization was determined using the formula mentioned in Ref. [47]. The uncertainty in the mixing ratio for the $R_{\rm DCO}$-polarization method was calculated by finding the range of $\tan^{-1}\delta$ for which the $\chi^2_{\rm min} + 1$ value is reached [42,48]. The values of the mixing ratio (δ) of the interconnecting transitions are tabulated in Table I.

IV. DISCUSSION

The $n_\omega = 0$ and 1 bands

As the Introduction points out, the wobbling motion in odd-A triaxial deformed nucleus occurs when the angular momentum (j) of the odd particle aligns with either of the principal axes of the triaxial core. When j of the odd quasiparticle is perpendicular (parallel) to the m axis, having the largest MoI, a transverse (longitudinal) mode of wobbling

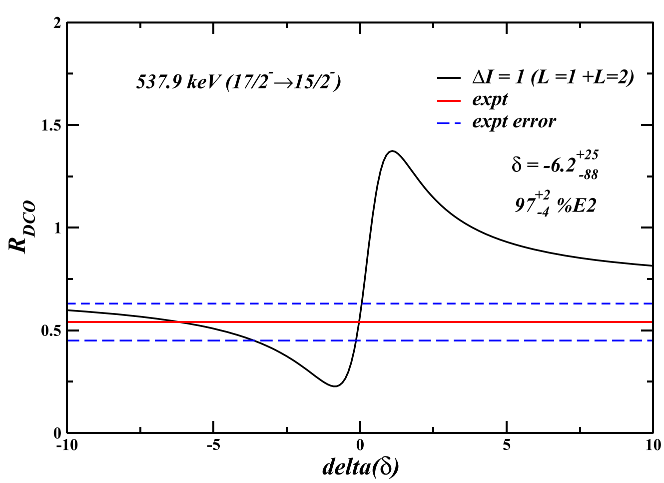

FIG. 7. The variation of $R_{\rm DCO}$ as a function of mixing ratio (δ) for 537.9-keV transition in ^{151}Eu giving two values of $\delta = -6.2^{+25}_{-88}$ and -0.04^{+9}_{-10}. The higher value of δ is mentioned in the plot as it is also supported by the polarization measurement.

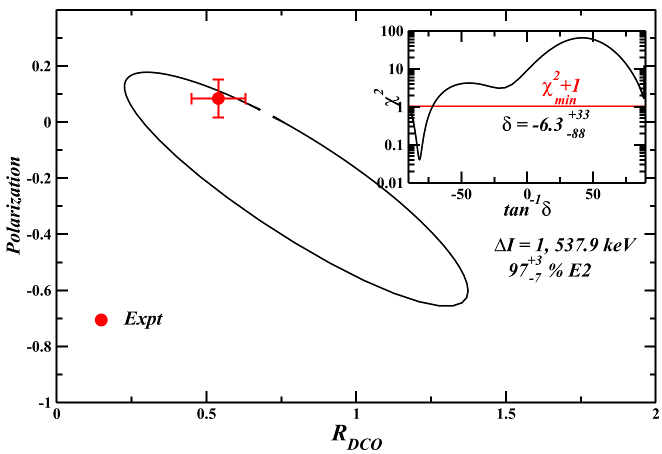

FIG. 8. The variation of R_{DCO} as a function of the polarization at different mixing ratio (δ) for 537.9-keV transition in ^{151}Eu in which the inset shows the minimum of the χ^2 versus $\tan^{-1}\delta$ plot giving mixing ratio $\delta = -6.3^{+33}_{-88}$. Here, the quoted negative uncertainty for δ is maximum probable uncertainty.

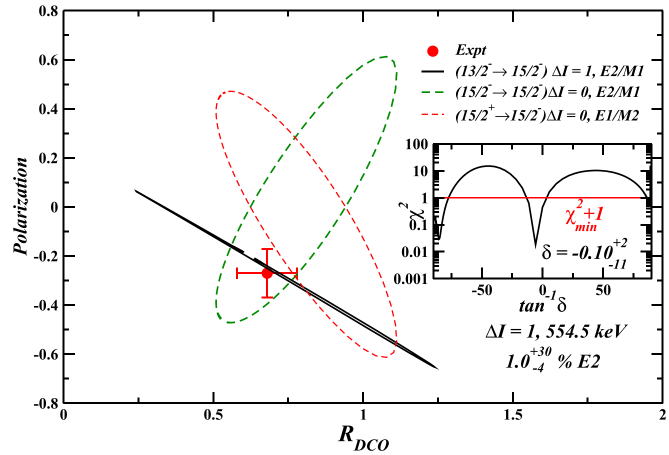

FIG. 10. The variation of R_{DCO} as a function of the polarization at different mixing ratio (δ) for 554.5-keV transition in ^{151}Eu in which the inset shows the minimum of the χ^2 versus $\tan^{-1}\delta$ plot giving mixing ratio $\delta = -0.10^{+2}_{-11}$.

motion is induced. The qualitative difference between the two modes of wobbling motion is given by the wobbling energy (E_{wobb}) defined as follows:

$$E_{\mathrm{wobb}} = E(I, n_\omega = 1) - \frac{E(I+1, n_\omega = 0) + E(I-1, n_\omega = 0)}{2}, \quad (6)$$

where n_ω is the wobbling phonon number and $E(I, n_\omega)$ is the excitation energy of the respective bands. The precession cone, defined by the rotor-, odd particle-, and total angular momenta, revolves around the m axis, which increases the wobbling energy E_{wobb} with increasing spin I in the case of the longitudinal wobbler. On the other hand, in the case of a transverse wobbler, the E_{wobb} decreases with an increase in I because of the revolution of the precession cone around the s (or l) axis, having smaller MoI relative to the m axis

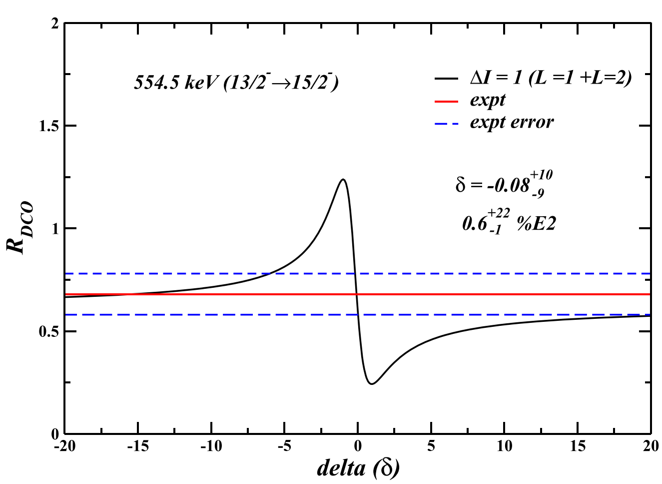

FIG. 9. The variation of R_{DCO} as a function of mixing ratio (δ) for 554.5-keV transition in ^{151}Eu giving $\delta = -0.08^{+10}_{-9}$.

[4]. Figure 11 shows the comparison of wobbling energy of ^{151}Eu nuclei with ^{135}Pr [11], ^{133}Ba [15], ^{133}La [13], ^{127}Xe [14], and ^{183,187}Au [4,16] nuclei where wobbling motion was established experimentally. As shown in Fig. 11(a), the wobbling energy gradually decreases with an increase in energy for ^{135}Pr, ^{133}Ba, and ^{183}Au isotopes showing the characteristics of transverse wobbling. In the case of the ^{135}Pr nucleus, the j of the quasiproton particle in the $h_{11/2}$ and in ^{183}Au the j of the quasiproton particle in the $i_{13/2}$ orbital aligns with the s axis of the triaxial core to produce the transverse mode of wobbling excitation. The contradictory increasing pattern of the wobbling energy for the positive parity band in ^{183}Au nucleus was suggested to be the initial part of the transverse wobbling band similar to the ^{163}Lu nucleus [16]. In the ^{133}Ba nucleus, the j of the quasineutron hole in the $h_{11/2}$ orbital aligns with the l axis to maximize its overlap with the triaxial core and behaves as a transverse wobbler. Similar to these established transverse wobblers, the wobbling energy of ^{151}Eu also decreases with increasing spin, indicating the presence of transverse wobbling in this nucleus. The j of the quasiparticle seems to align with the axis of the triaxial core to minimize the energy of its attractive short-range interaction leading to the occurrence of transverse wobbling motion. While in Fig. 11(b), the increasing wobbling energy as a function of spin (I) in ^{133}La, ^{127}Xe, and ^{187}Au shows the longitudinal wobbling motion of these isotopes. The alignment of j of the quasineutron particle in the $h_{11/2}$ orbital of ^{127}Xe and the quasiproton particle in the $i_{13/2}$ orbital of ^{187}Au with the m axis of the triaxial core causes the longitudinal mode of wobbling. Further, the theoretical comparison of wobbling motion in the ^{151}Eu nucleus with these established wobblers is discussed in terms of TPSM calculations in the next section.

One of the primary characteristics of wobbling motion is the appearance of rotational $E2$ bands from the excitation of the wobbling phonons n_ω, connected by strong $\Delta I = 1$ transitions having predominantly $E2$ character. In ^{151}Eu, the two rotational bands A and C are interconnected by $\Delta I = 1$

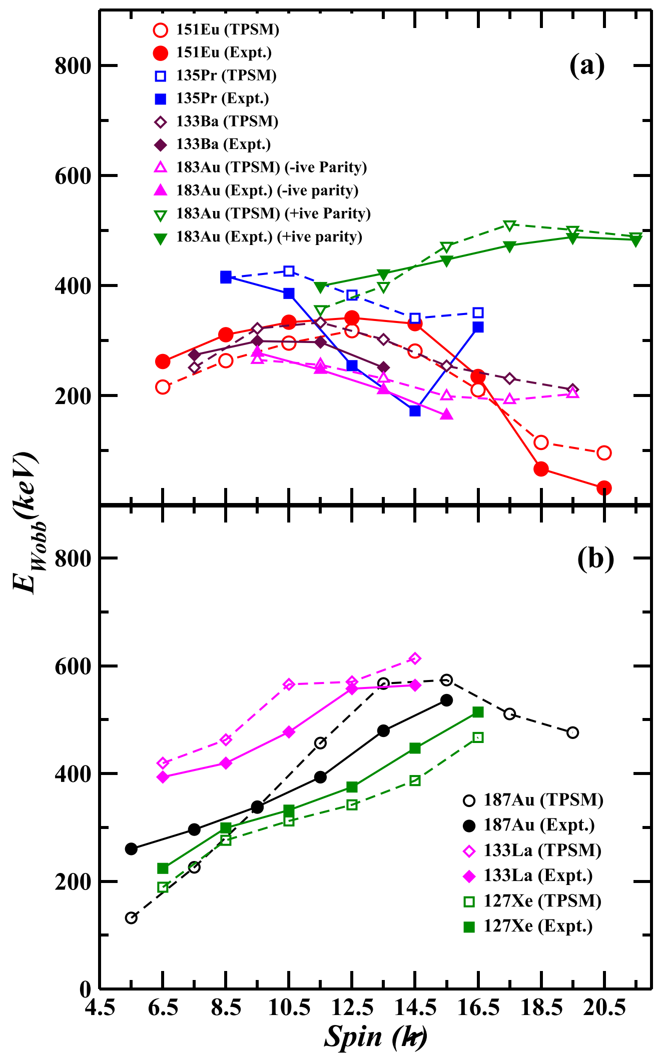

FIG. 11. Comparison of wobbling excitation energy for $n_\omega = 1$ band in ^{151}Eu with (a) transverse wobblers ^{135}Pr [11], ^{133}Ba [15], and ^{183}Au [16], and (b) longitudinal wobblers ^{187}Au [4], ^{133}La [13], and ^{127}Xe [14].

transitions. To determine the dominant $M1/E2$ character of these interlinking transitions R_{DCO} and linear polarization measurements have been carried out. The average mixing ratio $\delta_{\mathrm{av}} = -3.3^{+15}_{-33}$ for 415.0-keV transition, decaying from $13/2^- \rightarrow 11/2^-$, shows 91^{+7}_{-15}% of its $E2$ character. Whereas, $\delta_{\mathrm{av}} = -6.3^{+41}_{-88}$ for 537.9-keV transition, decaying from $17/2^- \rightarrow 15/2^-$, shows 97^{+3}_{-15}% of its $E2$ character. The comparison of calculated B(λL) ratios in ^{151}Eu with their corresponding counterparts in different triaxial nuclei showing wobbling motion is tabulated in Table III. The $\mathrm{B}(E2_{\mathrm{out}})/\mathrm{B}(E2_{\mathrm{in}})$ in ^{105}Pd, ^{135}Pr, and ^{133}Ba is larger than the $\mathrm{B}(M1_{\mathrm{out}})/\mathrm{B}(E2_{\mathrm{in}})$ for the $\Delta I = 1$ interconnecting transitions between the $n_\omega = 0$ and 1 bands, establishing their enhanced $E2$ character. Similarly, in the ^{151}Eu isotope, the higher values of $\mathrm{B}(E2_{\mathrm{out}})/\mathrm{B}(E2_{\mathrm{in}})$ for 415.0 and 537.9 keV supports band C as the wobbling band built from the excitation of $n_\omega = 1$ on the aligned $h_{11/2}$ proton configuration yrast band A (with

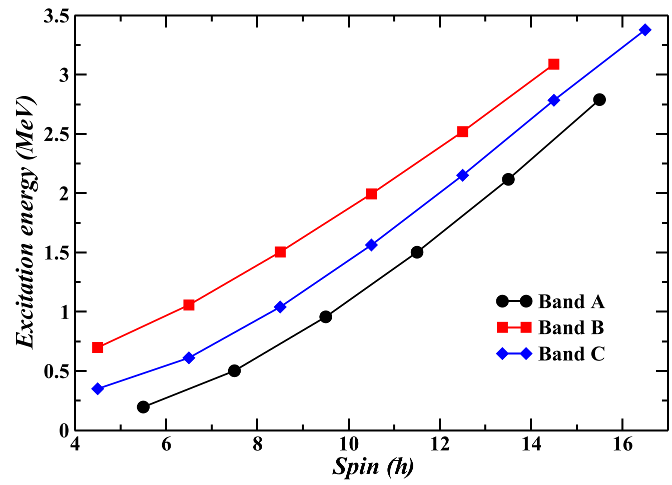

FIG. 12. The variation of excitation energy as a function of spin $I(\hbar)$ for bands A, B, and C of the ^{151}Eu isotope.

$n_\omega = 0$). Moreover, the increase in the % of the $E2$ character with spin is observed in ^{151}Eu similar to other wobbling nuclei as shown in Table III.

Another required characteristic to establish wobbling motion is the presence of the signature partner band of the $n_\omega = 0$ band connected by $\Delta I = 1$ transitions. It is essential to identify the signature partner band of the yrast $n_\omega = 0$ band to ensure that the band identified as the wobbler band is not misinterpreted as the signature partner band. Unlike the wobbling phonon band, the interband transitions between the zero phonon band and its signature partner should have a dominant $M1$ character. In the present study, three new interlinking transitions (554.5, 547.1, and 491.2 keV) have been placed between bands A and B in ^{151}Eu. The $\delta_{\mathrm{av}} = -0.09^{+11}_{-14}$ for 554.5-keV transition shows its dominant $M1$ character with only 0.8^{+42}_{-1}% $E2$ mixing. Similar to the signature partner bands of other wobbler nuclei, the higher value of $(M1_{\mathrm{out}})/\mathrm{B}(E2_{\mathrm{in}})$ for 554.5-keV transition in ^{151}Eu, supports band B as the unfavored signature partner (SP)of the $n_\omega = 0$ band A, as tabulated in Table III. Additionally, patterns of higher excitation energy and weak population in comparison to the $n_\omega = 1$ band are expected for the unfavored signature partner of the $n_\omega = 0$ bands. From the variation of excitation energy as a function of spin, shown in Fig. 12, it is noted that the excitation energy of band B is higher than that of band C, although both bands B and C are built on the $9/2^-$ state having similar spin sequence. Such observations further justify band B to be the signature partner of $n_\omega = 0$ band A.

V. TRIAXIAL PROJECTED SHELL MODEL ANALYSIS

In this section, we shall compare the experimental band structures and transition rates of ^{151}Eu with the numerical results obtained using the TPSM approach. The details of this formalism for odd-A nuclei can be found in Ref. [49], and the model was shown to be successful in describing the high spin states in ^{103,105}Rh [50], $^{125-137}$Pr, and $^{127-139}$Pm nuclei [51]. In the present case of ^{151}Eu, we have followed

TABLE III. The experimental mixing ratio (δ), $E2$ fractions, and experimentally obtained transition probability ratios $B(E2_{\mathrm{in}})/B(E2_{\mathrm{out}})$ and $B(M1_{\mathrm{in}})/B(E2_{\mathrm{out}})$, of various nuclei in comparison with the data for the ^{151}Eu nucleus.

Nucleus	E_γ(keV)	$I_i^\pi \to I_f^\pi$	δ[a]	E2%	$\frac{B(E2_{\mathrm{out}})}{B(E2_{\mathrm{in}})}$	$\frac{B(M1_{\mathrm{out}})}{B(E2_{\mathrm{in}})}(\mu_N^2/e^2b^2)$
$n_\omega = 1$ wobbling band						
^{151}Eu	415.0	$13/2^- \to 11/2^-$	-3.3^{+15}_{-33}	91^{+7}_{-15}	0.1836^{+124}_{-304}	0.0020^{+37}_{-15}
	537.9	$17/2^- \to 15/2^-$	$-6.3^{+41\mathrm{b}}_{-88}$	97^{+3}_{-15}	0.2795^{+58}_{-420}	0.0014^{+85}_{-12}
^{105}Pd [17]	991	$17/2^- \to 15/2^-$	1.8 ± 5	76 ±13	0.66 ± 18	0.16 2± 97
	1034	$21/2^- \to 19/2^-$	2.3 ±3	84 ±4	0.60 ±9	0.089 ± 26
	994	$25/2^- \to 23/2^-$	2.7 ±6	87 ±6	0.34 ±7	0.029 ±16
^{135}Pr [11]	812.8	$21/2^- \to 19/2^-$	−1.54 ±9	70.3 ±24	0.843 ±32	0.164 ±14
	754.6	$25/2^- \to 23/2^-$	−2.38 ±37	85.0 ±40	0.500 ±25	0.035 ± 9
^{133}Ba [15]	743.4	$17/2^- \to 15/2^-$	−2.10 ± 19	81.51 ±273	2.94 ±18	0.26 ±4
	812.0	$21/2^- \to 19/2^-$	−1.95 ±16	79.18 ±271	2.36 ±20	0.28 ± 4
Signature partner band						
^{151}Eu	554.5	$13/2^- \to 15/2^-$	-0.09^{+11}_{-14}	0.8^{+42}_{-1}	0.0014^{+72}_{-13}	0.0362^{+3}_{-15}
^{135}Pr [11]	593.9	$13/2^- \to 11/2^-$	−0.16 ±4	2.5 ±12	–	–
^{133}Ba [15]	1067.0	$13/2^- \to 11/2^-$	−0.15 ±2	2.20 ±57	–	–

[a]The average value of δ has been taken for the ^{151}Eu nucleus.
[b]The maximum probable negative uncertainty is mentioned for 537.9 keV.

the same approach with one proton quasiparticle state generated by solving the triaxial Nilsson potential and pairing the Hamiltonian solution obtained in the BCS approximation. The Nilsson potential with the deformation parameters ϵ and ϵ', listed in Table IV, have been used for ^{151}Eu and for other odd-A nuclei where wobbling motion has been identified. The axial deformation parameter ϵ is normally chosen from the measured quadrupole moment of the system, wherever available, otherwise the tabulated values using the phenomenological potential models are employed [4,13,16,17,52,53]. The value of ϵ' is, preferably, chosen from the minimum of the potential energy surface (PES) of the nucleus. However, for some nuclei, PES does not depict minimum, and for these nuclei the value of ϵ' that reproduces the wobbling band-head energy is adopted because it is known that this band-head energy is very sensitive to nonaxial deformation.

The intrinsic states obtained from the solution of the triaxial Nilsson potential with these deformation parameters are projected onto good angular-momentum states. For each state, about 40 to 50 intrinsic states are selected around the Fermi surface for which the angular-momentum projection is performed. These projected bands (basis states) were then employed to diagonalize the shell model Hamiltonian consisting of pairing and quadrupole-quadrupole interaction terms. The interaction strengths used in the present calculations are the same as those used in the previous studies [51]. The energies for the three bands, after the diagonalization, are shown in Fig. 13. It is quite evident from the figure that calculated values are in good agreement with the experimental data.

Using the semiclassical triaxial particle-rotor model [3,12] with irrotational-flow moment of inertia, it was shown that wobbling motion for odd systems can be categorized into longitudinal and transverse ones with angular momentum of the odd particle parallel and perpendicular to the medium axis. The main characteristic feature of longitudinal (transverse)

TABLE IV. The axial deformation parameter (ϵ), triaxial deformation parameter ϵ', and (γ) employed in the calculation for odd-A nuclei. The axial deformation ϵ is taken from Ref. [53]. The asterisk $*$ shows ϵ for positive parity in ^{183}Au nucleus.

	^{151}Eu	^{187}Au	^{135}Pr	^{133}La	^{127}Xe	^{133}Ba	^{183}Au	^{183}Au
ϵ	0.200	0.220	0.160	0.150	0.150	0.150	0.280	0.270*
ϵ'	0.110	0.100	0.110	0.110	0.100	0.100	0.110	0.100
γ^0	27	24	34	36	33	33	21	20

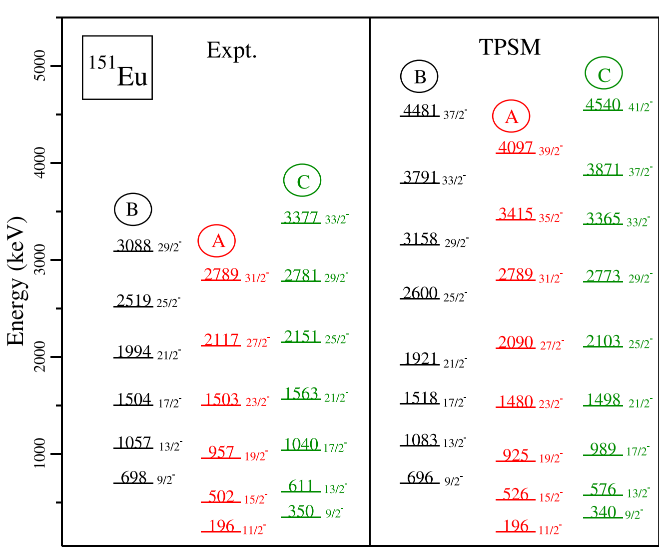

FIG. 13. Comparison of experimental levels with TPSM calculations.

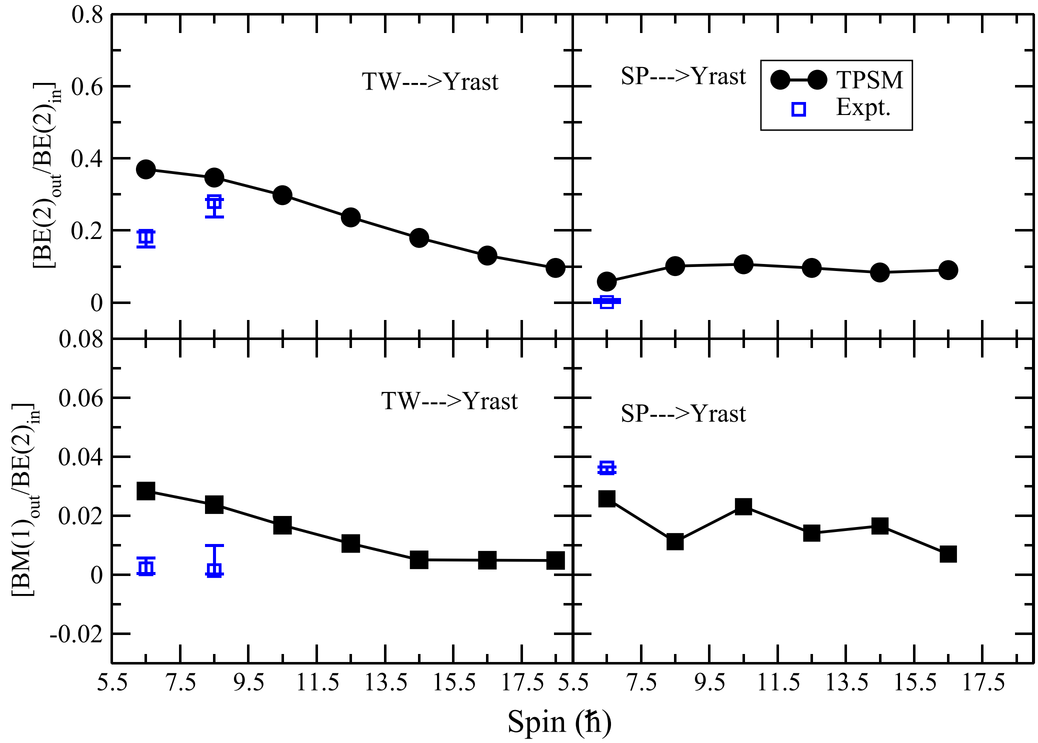

FIG. 14. B($E2_{\rm out}$)/B($E2_{\rm in}$) and B($M1_{\rm out}$)/B($E2_{\rm in}$) vs spin for the transverse wobbling band (TW); TW → yrast and signature partner band (SP); SP → yrast.

motion is that the wobbling frequency increases (decreases) with increasing angular momentum. In the microscopic TPSM approach, it is not possible to separate the core and the odd-particle angular momenta, and we adopt the semiclassical classification of these band structures.

The wobbling energies, $E_{\rm wobb}$, defined in Eq. (6), were calculated from the level energies and are plotted in Fig. 11 as a function of spin for the $n_\omega = 1$ band. The wobbling frequency decreases with angular momentum, which suggests a transverse wobbling motion in ^{151}Eu. It is observed from this figure that the results obtained using the TPSM approach are in good agreement with the experimental wobbling frequencies. In particular, the transverse nature of wobbling observed in ^{135}Pr, ^{133}Ba, and ^{183}Au and longitudinal wobbling in ^{187}Au, ^{133}La, and ^{127}Xe is well reproduced.

We have also evaluated the transition probabilities as they are very sensitive to the nature of the collective motion. The transition probabilities in the present case have been calculated [51] using free values of g_l, while g_s was attenuated by the 0.85 factor, i.e., $g_l^\pi = 1$, $g_l^\nu = 0$, $g_s^\pi = 5.59 \times 0.85$, and $g_s^\nu = -3.83 \times 0.85$. The effective charges for the protons and the neutrons were assumed to be 1.5e and 0.5e, respectively. A comparison of the experimental and the calculated transition probabilities for ^{151}Eu is shown in Fig. 14. It is known from the semiclassical analysis that the essential feature of the wobbling bands is that $E2$ transition probability dominates for the $n_\omega = 1 \to n_\omega = 0$ connecting transitions. In Fig. 14, we present the ratios of the transition probabilities B($E2_{\rm out}$)/B($E2_{\rm in}$) in the upper left panels and in the lower left panels B($M1_{\rm out}$)/B($E2_{\rm in}$) for these connecting transitions. The measured as well as calculated B($E2_{\rm out}$)/B($E2_{\rm in}$) ratios are large, indicating that the band exhibits the characteristics of wobbling motion. The results of transitions from SP → yrast are presented in the upper and lower right panels of Fig. 14 and the B($E2_{\rm out}$)/B($E2_{\rm in}$) ratios for these transitions are much smaller than those of LW → yrast linking transitions, which supports the interpretation of this structure as a signature partner band.

VI. SUMMARY

In the present study, the excited states of the ^{151}Eu nucleus have been investigated using ^{148}Nd(^{7}Li, 4n) ^{151}Eu reaction. The spin and parity of the bands are assigned using $R_{\rm DCO}$ and polarization measurements, respectively. Three new interconnecting transitions have been placed between the yrast band A and band B. The dominant $M1$ characteristic of the interconnecting $\Delta I = 1$, 554.5-keV transition, measured using experimental mixing ratio, along with the higher excitation energy, indicates band B to be the unfavored signature partner of the zero-phonon band A. While the dominant $E2$ behavior of the interconnecting $\Delta I = 1$ transitions between bands A and C suggests band C to be the $n_\omega = 1$ band built on the zero-phonon band A because of the first wobbling phonon excitation. Further, the decreasing wobbling excitation energy as a function of spin implies the ^{151}Eu nucleus to be the first candidate executing transverse wobbling motion in the $A \approx 150$ mass region. The experimental characteristic of the observed rotational bands was well described using the

TPSM approach. The calculated results support the transverse wobbling interpretation of bands A and C.

ACKNOWLEDGMENTS

The authors acknowledge the INGA collaboration for establishing the INGA array at IUAC, New Delhi. The authors thank the staff of the target laboratory for facilitating the preparation of the target and the Pelletron team for the smooth functioning of the accelerator at IUAC, New Delhi. A.M. and S.B. acknowledge financial support from IUAC (UFR-63314) and UGC-DAE-CSR (UGC-DAE-CSR-KC/CRS/19/NP04/0915), respectively. The authors (G.H.B., S.J., J.A.S., and N.R.) would like to acknowledge the Science and Engineering Research Board (SERB), Department of Science and Technology (Govt. of India) for providing financial assistance under Project No. CRG/2019/004960 to carry out a part of the present research work. A.K.J. acknowledges financial support from SERB Grant No. CRG/2020/000770.

[1] A. Bohr and B. R. Mottelson, *Nuclear Structure*, Vol. II (Benjamin, New York, 1975).
[2] I. Hamamoto, Phys. Rev. C **65**, 044305 (2002).
[3] S. Frauendorf and F. Donau, Phys. Rev. C **89**, 014322 (2014).
[4] N. Sensharma *et al.*, Phys. Rev. Lett. **124**, 052501 (2020).
[5] S. W. Ødegård *et al.*, Phys. Rev. Lett. **86**, 5866 (2001).
[6] P. Bringel *et al.*, Eur. Phys. J. A **24**, 167 (2005).
[7] D. R. Jensen *et al.*, Phys. Rev. Lett. **89**, 142503 (2002).
[8] G. Schönwaßer *et al.*, Phys. Lett. B **552**, 9 (2003).
[9] H. Amro *et al.*, Phys. Lett. B **553**, 197 (2003).
[10] D. J. Hartley *et al.*, Phys. Rev. C **80**, 041304(R) (2009).
[11] J. T. Matta *et al.*, Phys. Rev. Lett. **114**, 082501 (2015).
[12] N. Sensharma *et al.*, Phys. Lett. B **792**, 170 (2019).
[13] S. Biswas *et al.*, Eur. Phys. J. A **55**, 159 (2019).
[14] S. Chakraborty *et al.*, Phys. Lett. B **811**, 135854 (2020).
[15] K. Rojeeta Devi *et al.*, Phys. Lett. B **823**, 136756 (2021).
[16] S. Nandi *et al.*, Phys. Rev. Lett. **125**, 132501 (2020).
[17] J. Timar *et al.*, Phys. Rev. Lett. **122**, 062501 (2019).
[18] C. M. Petrache *et al.*, Phys. Lett. B **795**, 241 (2019).
[19] Q. B. Chen, S. Frauendorf, and C. M. Petrache, Phys. Rev. C **100**, 061301(R) (2019).
[20] F. Q. Chen and C. M. Petrache, Phys. Rev. C **103**, 064319 (2021).
[21] B. F. Lv *et al.*, Phys. Rev. C **105**, 034302 (2022).
[22] K. Tanabe and K. Sugawara-Tanabe, Phys. Rev. C **95**, 064315 (2017).
[23] E. A. Lawrie, O. Shirinda, and C. M. Petrache, Phys. Rev. C **101**, 034306 (2020).
[24] B. Qi, H. Zhang, S. Y. Wang, and Q. B. Chen, J. Phys. G: Nucl. Part. Phys. **48**, 055102 (2021).
[25] Q. B. Chen and S. Frauendorf, Eur. Phys. J. A **58**, 75 (2022).
[26] R. Budaca and C. M. Petrache, Phys. Rev. C **106**, 014313 (2022).
[27] K. Nomura and C. M. Petrache, Phys. Rev. C **105**, 024320 (2022).
[28] H. Jia, S. Y. Wang, B. Qi, C. Liu, and L. Zhu, Phys. Lett. B **833**, 137303 (2022).
[29] B. F. Lv *et al.*, Phys. Lett. B **824**, 136840 (2022).
[30] L. Hu, J. Peng, and Q. B. Chen, Phys. Rev. C **104**, 064325 (2021).
[31] J. R. Leigh *et al.*, J. Phys. G **3**, 519 (1977).
[32] J. R. Jongman *et al.*, Nucl. Phys. A **591**, 244 (1995).
[33] W. J. Vermeer *et al.*, Nucl. Phys. A **559**, 422 (1993).
[34] B. Singh, Nucl. Data Sheets **110**, 1 (2009).
[35] S. Muralithar *et al.*, Nucl. Instrum. Methods Phys. Res., Sect. A **622**, 281 (2010).
[36] R. K. Bhowmik, Ingasort Manual (private communication).
[37] D. C. Radford, Nucl. Instrum. Methods Phys. Res., Sect. A **361**, 297 (1995).
[38] D. C. Radford, Nucl. Instrum. Methods Phys. Res., Sect. A **361**, 306 (1995).
[39] R. Brun and F. Rademakers, Nucl. Instrum. Methods Phys. Res., Sect. A **389**, 81 (1997).
[40] S. Bhattacharya *et al.*, Phys. Rev. C **100**, 014315 (2019).
[41] E. S. Macias, W. D. Ruhter, D. C. Camp, and R. G. Lanier, Comput. Phys. Commun. **11**, 75 (1976).
[42] A. Mukherjee *et al.*, Phys. Rev. C **105**, 014322 (2022).
[43] P. M. Jones, Nucl. Instrum. Methods Phys. Res., Sect. A **362**, 556 (1995).
[44] O. Klein and Y. Nishina, Z. Phys. **52**, 853 (1929).
[45] C. Günther *et al.*, Phys. Rev. C **15**, 1298 (1977).
[46] G. F. Knoll, *Radiation Detection and Measurement*, 3rd ed. (Wiley, New York, 2009).
[47] J. R. Taylor, *An Introduction to Error Analysis: The Study of Uncertainties in Physical Measurements* (University Science Books Sausalito, California, 1997).
[48] S. Bhattacharya *et al.*, Phys. Rev. C **106**, 044312 (2022).
[49] G. H. Bhat, J. A. Sheikh, and R. Palit, Phys. Lett. B **707**, 250 (2012).
[50] G. H. Bhat, J. A. Sheikh, and R. Palit, Phys. Lett. B **738**, 218 (2014).
[51] S. Jehangir, G. H. Bhat, N. Rather, J. A. Sheikh, and R. Palit, Phys. Rev. C **104**, 044322 (2021).
[52] L. Hildingson, W. Klamra, T. Lindblad, C. G. Lindén, G. Sletten, and G. Sékely, Z. Phys. A **338**, 125 (1991).
[53] P. Moller, J. R. Nix, W. D. Myers, and W. J. Swiatecki, At. Data Nucl. Data Tables **59**, 185 (1995).